Research Article

Investigation of the Motion of a Spherical Object Located at Soft Elastic and Viscoelastic Material Interface for Identification of Material Properties

Hasan Koruk*
Faculty of Engineering, MEF University, Istanbul, Turkey
Department of Surgical and Interventional Engineering, School of Biomedical Engineering and Imaging Sciences, King's College London, London, United Kingdom

Antonios N. Pouliopoulos
Department of Surgical and Interventional Engineering, School of Biomedical Engineering and Imaging Sciences, King's College London, London, United Kingdom

* Corresponding author. E-mail: korukh@mef.edu.tr DOI: 10.14416/j.asep.2023.12.002
Received: 15 June 2023; Revised: 26 September 2023; Accepted: 30 October 2023; Published online: 12 December 2023

Abstract
Measuring the properties of soft viscoelastic materials is challenging. Here, the motion of a spherical object located at the soft elastic and viscoelastic material interface for the identification of material properties is thoroughly investigated. Formulations for different loading cases were derived. First, the theoretical models for a spherical object located at an elastic medium interface were derived, ignoring the medium viscosity. After summarizing the model for the force reducing to zero following the initial loading, we developed mathematical models for the force reducing to a lower non-zero value or increasing to a higher non-zero value, following the initial loading. Second, a similar derivation process was followed to evaluate the response of a spherical object located at a viscoelastic medium interface. Third, by performing systematic analyses, the theoretical models obtained via different approaches were compared and evaluated. Fourth, the measured and predicted responses of a spherical object located at a gelatin phantom interface were compared and the viscoelastic material properties were identified. It was seen that the frequency of oscillations of a spherical object located at the sample interface during loading was 10–15% different from that during unloading in the experimental studies here. The results showed that different loading cases have immense practical value and the formulations for different loading cases can provide an accurate determination of material properties in a multitude of biomedical and industrial applications.

Keywords: Dynamic Hertz model, Material properties, Shear modulus, Soft material, Sphere, Viscoelastic properties, Viscosity

1 Introduction

The dynamic response of a spherical object, such as a bubble and a sphere, placed inside a medium [1]–[7] and located at a medium interface [8]–[14] has been investigated to identify material properties and understand the dynamics of soft structures. Creating or placing a spherical object inside a medium is difficult and can change the medium material properties. Thus, the experimental setup using a spherical object located at a medium interface is more convenient for the determination of material properties in practical applications [15]. Furthermore, as bubbles are not stable and their manipulation during experiments is difficult, a non-deformable spherical object located at a medium interface is more practical for evaluating material properties [14]. It should be noted that, unlike other parameters such as shear modulus, the accurate

modeling and experimentally identification of damping or viscosity for almost any type of material is always challenging, as many parameters affect the damping of a system [11], [16]–[19]. Therefore, measuring the properties of soft viscoelastic materials that exhibit both viscous and elastic characteristics when undergoing deformation is challenging.

There are some research studies on the identification of material properties based on the displacement of a sphere located at the material interface. Many of these studies are for static loading, and they only provide material elastic properties, such as the shear modulus or Young's modulus [20]–[24]. Some studies focus on the steady-state deformation of the sphere or relaxation, rather than on the measurement of vibrations of the spherical object located at the sample interface [25]–[27]. The models for an object located at a viscoelastic medium interface in the literature are complicated and may not provide the correct viscoelastic properties of the test sample. For example, Mizukami *et al.* [28] designed a test rig to determine the elastic and viscous parameters of the contact interface based on resonance shear measurement. In their setup, they placed a hard sphere on a hydrogel. The sphere was connected to a four-sectored piezo tube and hung by a pair of vertical springs. The hydrogel was mounted on a plate, which was connected to a horizontal double-cantilever spring. This complicated system contains the parameters of many other components, and the elastic and viscous parameters of the contact interface were determined, not the viscosity of the hydrogel.

There are some attempts to obtain mathematical models for the oscillations of a sphere placed on a half-space [29]–[31]. However, in these studies, the medium viscosity of the medium is not considered [29], the excitation is assumed to be a rectangular pulse with zero amplitude at the start and end of the function [30], [31] and the period of oscillations is assumed to be the same in the loading and relaxation phases [30]–[32]. Therefore, there is a need to establish a practical test rig and develop an accurate mathematical model for the dynamic response of a spherical object located at a medium interface exposed to an external force. This model should work for different loading cases encountered in practical applications, as explained in more detail in the next two paragraphs.

The excitation as a rectangular pulse is common in practice [2], [7]. In this approach, a force is applied for a duration of time, and after that the force is removed as seen in Figure 1(a) (i.e., $\overline{F}_1 > 0$ for $0 \le t \le \tau$ and $\overline{F}_2 = 0$ for $t > \tau$). It should be noted that mathematical models for a sphere located at the interface of an elastic medium [30] and placed at the interface of a viscoelastic medium [31] exposed to a rectangular pulse seen in Figure 1(a) have recently been proposed. It should be noted that the mathematical model in [31] has recently been updated for a trapezoidal pulsed force in [32]. However, in practical applications, due to the mass of the spherical object, the force in the second phase is not zero as depicted in Figure 1(b) (i.e., $\overline{F}_1 > 0$ for $0 \le t \le \tau$ and $\overline{F}_1 > \overline{F}_2 \ne 0$ for $t > \tau$). Furthermore, the medium is first deformed by the weight of the spherical object, and then the external force is applied in practice as illustrated in Figure 1(c) (i.e., $\overline{F}_1 > 0$ for $0 \le t \le \tau$ and $\overline{F}_2 > \overline{F}_1 \ne 0$ for $t > \tau$). A practical loading case is the combination of Figures 1(b) and (c) in which the external force is applied following the initial static loading and the external force is removed in the next step as shown in Figure 1(d). Therefore, in addition to the force applied to the spherical object, the weight of the spherical object (or any other forces in the system) should be considered in the mathematical model. Especially for soft materials, the weight of the spherical object cannot be ignored. The weight of the spherical object can be even greater than the applied force in practical applications, hence it should be taken into consideration. Furthermore, the frequency of oscillations is assumed to be the same in the loading and relaxation phases in the previous proposed mathematical models [30]–[32]. However, the stiffness of the system consisting of a spherical object located at a medium interface depends on the external force and the inertia of the medium involved in motion changes with the sphere displacement (or the external force). As a result, the frequency of oscillation is expected to change when there is a change in the external force. Therefore, mathematical models for a spherical object located at the medium interface for the practical loading cases given in Figure 1(b) and (c) were developed in this study. Furthermore, the proposed mathematical models in this paper simulate the change in the frequency of oscillations due to the change in the external force. We believe that these mathematical models can be

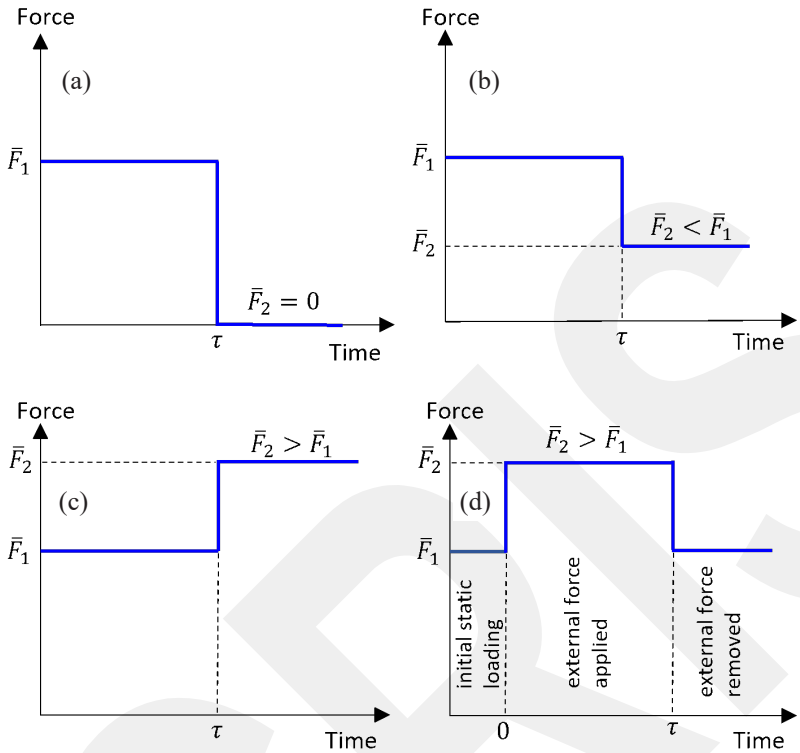

Figure 1: Different loading cases: (a) The case in which a force is applied for a time duration τ and then removed. (b) The case in which the force in the second phase is not zero. (c) The case in which the medium is first deformed by the weight of the spherical object and then the external force is applied. (d) A practical loading case in which the external force is applied following the initial static loading and the external force is removed in the next step.

widely used for the identification of material properties and for understanding the dynamics of soft structures in practical applications. Here, in addition to presenting mathematical models for different practical loading cases and evaluating their performance, the mathematical model for a spherical object located at a viscoelastic medium interface was evaluated using an experimental study.

Because the weight of the spherical object is not negligible for soft material applications, the formulations for the loading case in Figure 1(b) provide an accurate determination of material properties. The force during unloading should be greater than zero or large enough to maintain contact between the sphere and medium. Therefore, the loading depicted in Figure 1(c) is a desired loading case in practical applications. It should be noted that the practical loading case in Figure 1(d) is the combination of the loading cases in Figure 1(b) and (c). Although only the loading phase was considered in the previous studies [14], [15], [32], both loading and unloading phases were used to identify material properties and/or to further confirm the identified material properties in this study. To our best knowledge, this is the first study that experimentally and theoretically evaluates the characteristics of the vibration of a spherical object located at a soft material interface and shows that its frequencies of oscillations are different in the loading and unloading phases. In addition, the mathematical model proposed in this study considers the radiation damping due to the change in the external force and the inertia of the medium involved in motion.

The structure of this paper is as follows. By ignoring the medium viscosity, the theoretical models for a spherical object located at an elastic medium interface are presented in Section 2. Here, after

summarizing the model for the force reducing to zero following the initial loading [Figure 1(a)], the models for the force reducing to a lower non-zero value [Figure 1(b)] or increasing to a higher non-zero value [Figure 1(c)] following the initial loading were developed. A similar derivation process was followed to evaluate the response of a spherical object located at a viscoelastic medium interface in Section 3. By performing systematic analyses, the theoretical models obtained via different approaches were compared and evaluated in Section 4. Some experiments were performed using a spherical object located at a soft material (gelatin phantom) interface. Here, an electromagnet was used to apply the force to the spherical object and a high-speed camera was used to track the movement of the spherical object. The measured and predicted responses of the spherical object located at the gelatin phantom were compared and the viscoelastic material properties were identified in Section 5. The main outcomes of this study are summarized in Section 6.

2 Theoretical Models for Spherical Object Located at Elastic Medium Interface

2.1 *Force reducing to zero following initial loading* ($\bar{F}_1 > 0$, $\bar{F}_2 = 0$, Figure 1(a))

An analytical model for the dynamic response of a non-deformable sphere located at an elastic medium interface was proposed in 2021 [30]. In addition to considering the elastic properties of the medium and the size of the sphere, this model considers the density of the medium (i.e., the inertia of the medium involved in motion), the mass of the sphere (the inertia of the sphere), and the radiation damping due to shear waves. This model can be used for both small and large sphere displacements. The model in [30] was corrected for the Poisson's ratio of the medium of $\nu = 0.45$. Later, based on a number of finite element analyses, a mathematical model for all practical Poisson's ratios of the medium was suggested in 2022 [31]. Hence, for the loading in Figure 1(a), using the references [30] and [31], the response of the spherical object located at the elastic medium interface for the initial loading (first phase, $\bar{F}_1 = \bar{F} > 0$ for $0 \le t \le \tau$) and the relaxation (second phase, $\bar{F}_2 = 0$ for $t > \tau$) can be written as following Equations (1) and (2):

$$u_1(t) = \frac{f}{k} - \frac{f}{k\sqrt{1-\zeta^2}} e^{-\zeta\omega_n t} \cos(\omega_d t - \varphi) \text{ for } 0 \le t \le \tau \quad (1)$$

$$u_2(t) = \frac{f e^{-\zeta\omega_n t}}{k\sqrt{1-\zeta^2}} \left\{ e^{\zeta\omega_n \tau} \cos\left[\omega_d (t-\tau) - \varphi\right] - \cos(\omega_d t - \varphi) \right\} \text{ for } t > \tau \quad (2)$$

where the subscripts 1 and 2 denote the first (loading) and second (unloading) phases, respectively, f is the effective force, k is the equivalent stiffness coefficient, ζ is the equivalent damping ratio due to radiation damping, ω_n is the undamped natural frequency, ω_d is the damped natural frequency, and φ is the phase angle. The expressions needed in Equations (1) and (2) are given in Equations (3)–(15) [30], [31]:

$$f = \left[1 + 0.5\left(1 - \alpha \frac{\bar{U}}{R} \right) \right] \bar{F} \quad (3)$$

$$k = \left(1 - \alpha \frac{\bar{U}}{R} \right) 1.5 \left(\frac{4E^* \sqrt{R}}{3} \right)^{2/3} \bar{F}^{1/3} \quad (4)$$

$$\zeta = \frac{c}{c_{cr}} = \frac{c}{2\sqrt{km}} \quad (5)$$

$$\omega_n = \sqrt{\frac{k}{m}} \quad (6)$$

$$\omega_d = \omega_n \sqrt{1-\zeta^2} \quad (7)$$

$$\varphi = \tan^{-1} \frac{\zeta}{\sqrt{1-\zeta^2}} \quad (8)$$

where

$$E^* = \frac{E}{1-\nu^2} \quad (9)$$

$$E = 2G(1+\nu) \quad (10)$$

$$\bar{U} = \left(\frac{3\bar{F}}{4E^* \sqrt{R}} \right)^{2/3} \tag{11}$$

$$\alpha = \nu - 0.35 \tag{12}$$

$$\beta = 0.5 \tag{13}$$

$$c = \frac{1}{2}\left(\beta + \frac{\bar{U}}{R} \right)\left(\sqrt{\frac{\rho}{G}} R \right)\left(1 - \alpha \frac{\bar{U}}{R} \right) 1.5 \bar{F}^{1/3} \left(\frac{4E^* \sqrt{R}}{3} \right)^{2/3} \tag{14}$$

$$m = \frac{1}{3}\pi R^3 \left(a\rho_s + \frac{\bar{U}}{R}\rho \right) \tag{15}$$

where $a = 4$ for a sphere and $a = 2$ for a hemisphere. Here, $\bar{U}$ is the static displacement of the spherical object, $\bar{F}$ and τ are the amplitude and excitation duration of the applied force, G, E, ρ, and ν are the shear modulus, Young's modulus, density, and Poisson's ratio of the medium material, R and ρ_s are the radius and density of the spherical object, E^* is the reduced Young's modulus of the spherical object located at the medium interface, c is the equivalent damping coefficient due to radiation damping, c_{cr} is the corresponding critical damping coefficient, and m is the effective mass of the system including the mass of the spherical object and the mass of the sample involved in motion. In this study, the magnitude of the applied force $\bar{F}$ is the sum of the magnitude of the applied magnetic force ($\bar{F}_m$) and the weight of the spherical object ($\bar{F}_w$) given in Equation (16):

$$\bar{F} = \bar{F}_m + \bar{F}_w \tag{16}$$

It should be noted that the frequency of oscillations is assumed to be the same in the loading and relaxation phases in this model.

2.2 *Force reducing to a lower non-zero value following initial loading* ($\bar{F}_1 > \bar{F}_2 \neq 0$, Figure 1(b))

The model summarized in Section 2.1 is extended for a non-zero force lower than the initial load (i.e., $\bar{F}_2 < \bar{F}_1$, see Figure 1(b)) in this study. For the initial loading phase, the response will be the same as in Equation (1) and can be written as following Equation (17):

$$u_1(t) = \frac{f_1}{k_1} - \frac{f_1}{k_1\sqrt{1-\zeta_1^2}} e^{-\zeta_1 \omega_{n,1} t} \cos(\omega_{d,1} t - \varphi_1)$$
$$\text{for } 0 \le t \le \tau \tag{17}$$

Using $\bar{F} = \bar{F}_1 = \bar{F}_m + \bar{F}_w$, all parameters needed in Equation (17) can be calculated using the expressions presented in Section 2.1. As stated before, the subscript 1 denotes the first (loading) phase.

In contrast to Section 2.1, where the amplitude of the force in the relaxation phase is zero, the magnitude of the force is $\bar{F} = \bar{F}_2$ in the second phase this time. The external force is equal to the weight of the spherical object, i.e., $\bar{F}_2 = \bar{F}_w$, in this study. The response of the spherical located at the sample interface in the second phase is determined by exploiting the free vibrations of a system. Here, the response of the spherical object at $t = \tau$ predicted using Equation (17) is used as an initial condition. Hence, the response of the spherical object at the sample interface in the second phase can be determined using (Equation (18)):

$$u_2(t) = \bar{U}_2 + Ae^{-\zeta_2 \omega_{n,2}(t-\tau)} \sin\left[\omega_{d,2}(t-\tau) + \varphi_2\right] \text{ for } t > \tau \tag{18}$$

where $\bar{U}_2$ is the static displacement of the spherical object due to $\bar{F}_2$, and A and φ_2 are some constants to be determined from the initial conditions using the following using Equations (19) and (20) [33]:

$$A = \sqrt{\frac{(V_0 + \zeta_2 \omega_{n,2} X_0)^2 + (\omega_{d,2} X_0)^2}{\omega_{d,2}^2}} \tag{19}$$

$$\varphi_2 = \tan^{-1}\left(\frac{\omega_{d,2} X_0}{V_0 + \zeta_2 \omega_{n,2} X_0} \right) \tag{20}$$

Here, X_0 and V_0 are the displacement and velocity of the spherical object at $t = \tau$. It should be noted that $X_0 = -(\bar{U}_1 - \bar{U}_2)$ and $V_0 = 0$ at the steady-state position ($\bar{U}_1$ and $\bar{U}_2$ can be calculated using $\bar{F} = \bar{F}_1$ and $\bar{F} = \bar{F}_2$ in Equation (11), respectively). All other parameters needed in Equations (18)–(20) can be calculated using $\bar{F} = \bar{F}_2$ in the expressions presented in Section 2.1.

2.3 *Force increasing to a higher non-zero value following initial loading* ($\bar{F}_1 < \bar{F}_2$, Figure 1(c))

The formulation for the force increasing to a higher non-zero value following initial loading (i.e., $\bar{F}_1 < \bar{F}_2$) is the same as the formulation presented in Section 2.2. However, different from Section 2.2, $\bar{F}_1$ is equal to the weight of the spherical object and $\bar{F}_2$ equals the sum of the weight of the spherical object and external force this time. It should be noted that this system has high practical significance.

3 Theoretical Models for Spherical Object Located at Viscoelastic Medium Interface

3.1 *Force reducing to zero following initial loading* ($\bar{F}_1 > 0$, $\bar{F}_2 = 0$, Figure 1(a))

A comprehensive mathematical model for the dynamic response of a sphere located at a viscoelastic medium interface was proposed in 2022 [31]. Hence, for the loading in Figure 1(a) (i.e., $\bar{F}_1 = \bar{F} > 0$ for $0 \le t \le \tau$ and $\bar{F}_2 = 0$ for $t > \tau$), the dynamic response of a sphere and hemisphere located at the viscoelastic interface is found using the inverse Fourier transform and can be rewritten as Equation (21) [31]:

$$u(t)=\frac{1}{2\pi}\int_{-\infty}^{\infty}\frac{\left\{1+0.5\left(1-\alpha\frac{\bar{U}}{R}\right)\right\}\left[-\frac{j\bar{F}}{\omega}(e^{j\omega\tau}-1)\right]e^{-j\omega t}}{\frac{1}{3}\pi R^3\left(a\rho_s+\frac{\bar{U}}{R}\rho\right)(-\omega^2)+\left[\frac{1}{2}\left(\beta+\frac{\bar{U}}{R}\right)\left(\sqrt{\frac{\rho}{G-j\omega\eta}}R\right)(-j\omega)+1\right]\left(1-\alpha\frac{\bar{U}}{R}\right)1.5\bar{F}^{1/3}\left(\frac{4\tilde{E}^*\sqrt{R}}{3}\right)^{2/3}}d\omega \quad (21)$$

where η is the viscosity of the medium, $a = 4$ for a sphere and $a = 2$ for a hemisphere, ω is the angular frequency, and the reduced Young's modulus for a viscous sample is given in Equation (22):

$$\tilde{E}^*=\frac{2(G-j\omega\eta)(1+\nu)}{1-\nu^2} \quad (22)$$

The response of the spherical object for the loading and relaxation phases are $u_1(t) = u(t = 0 \rightarrow \tau)$ and $u_2(t) = u(t > \tau)$. The expressions for α and $\bar{U}$ and the values for β are given in Section 2.1. The frequency of oscillations is assumed to be the same in the loading and relaxation phases in this model.

3.2 *Force reducing to a lower non-zero value following initial loading* ($\bar{F}_1 > \bar{F}_2 \neq 0$, Figure 1(b))

The model summarized in Section 3.1 was extended for a non-zero force lower than the initial load (i.e., $\bar{F}_2 < \bar{F}_1$, see Figure 1(b)) in this study. For the loading phase, $\bar{F} = \bar{F}_1$ and $\bar{U} = \bar{U}_1$ are used for $t = 0 \rightarrow \tau$ in Equation (21) as given in Equation (23).

By considering $\bar{U} = \bar{U}_2$ and the change in force in the relaxation phase for $t > \tau$ in Equation (21), the response of the spherical object in the second phase can be written as given in Equation (24).

$$u_1(t)=\frac{1}{2\pi}\int_{-\infty}^{\infty}\frac{\left\{1+0.5\left(1-\alpha\frac{\bar{U}_1}{R}\right)\right\}\left[-\frac{j\bar{F}_1}{\omega}(e^{j\omega\tau}-1)\right]e^{-j\omega t}}{\frac{1}{3}\pi R^3\left(a\rho_s+\frac{\bar{U}_1}{R}\rho\right)(-\omega^2)+\left[\frac{1}{2}\left(\beta+\frac{\bar{U}_1}{R}\right)\left(\sqrt{\frac{\rho}{G-j\omega\eta}}R\right)(-j\omega)+1\right]\left(1-\alpha\frac{\bar{U}_1}{R}\right)1.5\bar{F}_1^{1/3}\left(\frac{4\tilde{E}^*\sqrt{R}}{3}\right)^{2/3}}d\omega$$

for $0 \le t \le \tau$ (23)

$$u_2(t)=\bar{U}_2+\frac{1}{2\pi}\int_{-\infty}^{\infty}\frac{\left\{1+0.5\left(1-\alpha\frac{\bar{U}_2}{R}\right)\right\}\left[-\frac{j\Delta\bar{F}}{\omega}(e^{j\omega\tau}-1)\right]e^{-j\omega t}}{\frac{1}{3}\pi R^3\left(a\rho_s+\frac{\bar{U}_2}{R}\rho\right)(-\omega^2)+\left[\frac{1}{2}\left(\beta+\frac{\bar{U}_2}{R}\right)\left(\sqrt{\frac{\rho}{G-j\omega\eta}}R\right)(-j\omega)+1\right]\left(1-\alpha\frac{\bar{U}_2}{R}\right)1.5\bar{F}_2^{1/3}\left(\frac{4\tilde{E}^*\sqrt{R}}{3}\right)^{2/3}}d\omega$$

for $t > \tau$ (24)

where $\Delta\overline{F} = \overline{F}_1 - \overline{F}_2$. The external force in the second phase is equal to the weight of the spherical object, i.e., $\overline{F}_2 = \overline{F}_w$, in this study.

3.3 *Force increasing to a higher non-zero value following initial loading* ($\overline{F}_1 < \overline{F}_2$, Figure 1(c))

The formulation for the force increasing to a higher non-zero value following initial loading (i.e., $\overline{F}_1 < \overline{F}_2$) is the same as the formulation presented in Section 3.2. However, in contrast to Section 3.2, $\overline{F}_1$ is equal to the weight of the spherical object while $\overline{F}_2$ equals the sum of the weight of the spherical object and external force this time. As stated before, this system has high practical significance.

4 Evaluation of the Theoretical Models

The response of a spherical object located at an elastic medium interface with no viscosity was modeled by exploiting the forced vibrations of a system in the loading phase and the free vibrations of a system in the relaxation phase in Section 2. The response of a spherical object located at a viscoelastic medium interface was determined by solving the equation of motion written in the frequency domain using the inverse Fourier transform in Section 3. These two different approaches were compared by taking the medium viscosity as zero in the models for the viscoelastic medium presented in Section 3.

The two approaches for the force reducing to zero following the initial loading ($\overline{F}_1$ = 2 mN for $0 \le t \le \tau$ = 100 ms and $\overline{F}_2$ = 0 for τ > 100 ms) are compared in Figure 2 for the sample input parameters that are similar to the ones used in practical applications [2], [11], [20], [34]. It is seen that both approaches produce the same results for the loading phase, while there are some small differences in the amplitudes after the load is removed in the relaxation phase. The period of oscillations is 9.95 ms (or the frequency of oscillations is 100.50 Hz) for the loading and relaxation phases for both approaches.

The two approaches for the force reduced to a lower non-zero value following the initial loading ($\overline{F}_1$ = 2.0 mN for $0 \le t \le \tau$ = 100 ms and $\overline{F}_2$ = 1.5 mN for τ > 100 ms) are compared in Figure 3(a) using the same parameters used in Figure 2. It is seen that both approaches produce the same results for the first

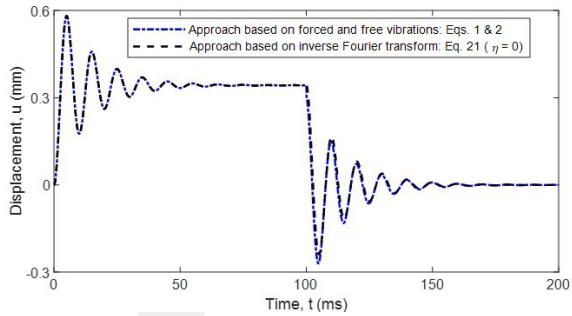

Figure 2: Comparison of the two approaches for the force reducing to zero following the initial loading ($\overline{F}_1$ = 2 mN for $0 \le t \le \tau$ = 100 ms and $\overline{F}_2$ = 0 for τ > 100 ms). Blue dash-dot curve: The response of a spherical object located at an elastic medium interface predicted by the model exploiting the forced vibrations of a system in the loading phase and free vibrations of a system in the relaxation phase [Equations (1) and (2)]. Black dashed curve: The response of a spherical object located at a viscoelastic medium interface determined by solving the equation of motion written in the frequency domain using the inverse Fourier transform [Equation (21)]. Medium and sphere properties: G = 2000 Pa, ρ = 1500 kg/m^3, η = 0, ν = 0.49, R = 1 mm and ρ_s = 5000 kg/m^3.

loading phase, while there are some small differences in the amplitudes, especially after the load is removed in the second phase. The effect of discontinuity of the force is clearly seen, just after the force is decreased. The period of oscillations is 9.95 ms (or the frequency of oscillations is 100.50 Hz) for the loading phase. However, the period of oscillations is estimated to be 10.40 ms (or the frequency of oscillations is 96.20 Hz) by both approaches in the second phase. The frequency of oscillations decreases from 100.50 to 96.20 Hz when the load is reduced from 2.0 to 1.5 mN. As the stiffness of the system decreases with decreasing load, the frequency of oscillations is decreased when the load is reduced from 2 to 1.5 mN, as expected.

Similarly, the two approaches for the force increasing to a higher non-zero value following the initial loading ($\overline{F}_1$ = 2 mN for $0 \le t \le \tau$ = 100 ms and $\overline{F}_2$ = 2.5 mN for τ > 100 ms) are compared in Figure 3(b) using the same parameters used in Figure 2 [or Figure 3(a)]. It is seen that, as the stiffness of the system increases with increasing load, the frequency of

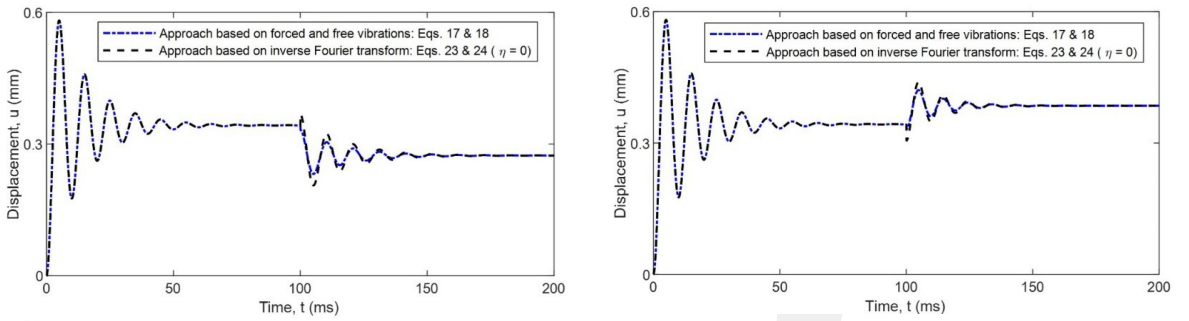

Figure 3: Comparison of the two approaches (a) for the force reducing to a lower non-zero value following the initial loading ($\overline{F}_1$ = 2.0 mN for $0 \le t \le \tau$ = 100 ms and $\overline{F}_2$ = 1.5 mN for τ > 100 ms) and (b) for the force increasing to a higher non-zero value following the initial loading ($\overline{F}_1$ = 2.0 mN for $0 \le t \le \tau$ = 100 ms and $\overline{F}_2$ = 2.5 mN for τ > 100 ms). Blue dash-dot curve: The response of a spherical object located at an elastic medium interface predicted by the model exploiting the forced vibrations of a system in the loading phase and the free vibrations of a system in the relaxation phase [Equations (17) and (18)]. Black dashed curve: The response of a spherical object located at the viscoelastic medium interface determined by solving the equation of motion written in the frequency domain using the inverse Fourier transform [Equations (23) and (24)]. Medium and sphere properties: G = 2000 Pa, ρ = 1500 kg/m^3, η = 0, ν = 0.49, R = 1 mm and ρ_s = 5000 kg/m^3.

oscillations is increased from 100.50 to 103.09 Hz (or the period of oscillations decreases from 9.95 to 9.70 ms) when the load is increased from 2.0 to 2.5 mN.

It is seen in Figures 2 and 3 that the steady-state displacement of the sphere is 0.34 mm in the initial phase for a force $\overline{F}_1$ = 2.0 mN. As seen in Figure 2, the steady-state displacement of the sphere reduces to zero in the relaxation phase at the end, as the load is completely removed (i.e., $\overline{F}_2$ = 0). However, as seen in Figure 3(a), the steady-state displacement of the sphere in the second phase reduces to 0.27 mm, as the load is not completely removed, it is reduced to a lower value (i.e., $\overline{F}_2$ = 1.5 mN). Similarly, as can be seen in Figure 3(b), the steady-state displacement of the sphere in the second phase increases to 0.39 mm, as the load is increased to a higher value (i.e., $\overline{F}_2$ = 2.5 mN).

It should be noted that the viscosity of the sample is assumed to be zero (i.e., no material damping) in the results presented in Figures 2 and 3. The decay of the response in Figures 2 and 3 is due to the radiation damping. The results show that the effect of radiation damping can be significant and should be considered in practical applications. In contrast to the approach based on the forced vibrations of a system in the first phase and the free vibrations of a system in the second phase to model elastic samples, the approach based on the inverse Fourier transform to model viscoelastic samples can simulate practical applications. Overall, the approach based on the forced vibrations of a system in the first phase and the free vibrations of a system in the second phase validated the other model, at least for the special case of no sample viscosity. Based on the literature on the dynamic response of damped systems [35]–[39], the amplitudes of oscillations should decrease, the steady-state displacement should not change, the frequency of oscillations should slightly decrease, and the reaction time should increase with increasing damping or viscosity of the system. In the following, the proposed mathematical model for the response of a spherical object located at the interface of a viscoelastic medium was assessed, by taking into account these facts. The response of a spherical object located at the interface of a viscoelastic sample with different viscosities determined by solving the equation of motion written in the frequency domain using the inverse Fourier transform [Equations (17) and (18)] is plotted in Figure 4. As more energy is dissipated during the oscillation of the spherical object located at the interface of the medium with higher viscosity, the amplitudes of oscillations of the sphere decrease with increasing medium viscosity both in the first and second phases. On the other hand, as the applied force and the internal stiffness force balance each other at the steady state, the medium viscosity does not change

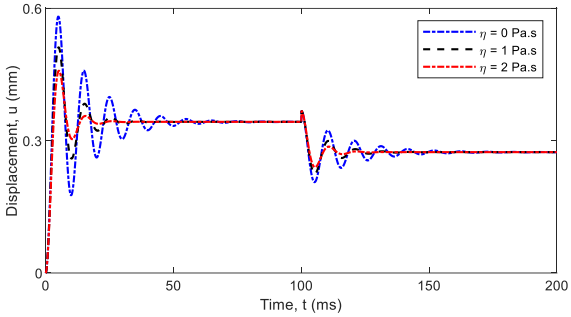

Figure 4: The response of a spherical object located at the interface of a viscoelastic sample with different viscosities determined by solving the equation of motion written in the frequency domain using the inverse Fourier transform [Equations (23) and (24)]. Loading: $\overline{F}_1$ = 2.0 mN for $0 \le t \le \tau$ = 100 ms and $\overline{F}_2$ = 1.5 mN for τ > 100 ms. Medium and sphere properties: G = 2000 Pa, ρ = 1500 kg/m^3, ν = 0.49, R = 1 mm and ρ_s = 5000 kg/m^3.

the steady-state displacement of the sphere both in the first and second phases. The period of oscillations is 9.95, 10.15 and 10.35 ms (or the frequency of oscillations is 100.50, 98.52, and 96.62 Hz) in the first phase when the medium viscosity is η = 0, 1, and 2 Pa·s, respectively. Similarly, the period of oscillations is 10.40, 10.55, and 10.75 ms (or the frequency of oscillations is 96.15, 94.79, and 93.02 Hz) in the second phase when the medium viscosity is η = 0, 1, and 2 Pa·s, respectively. Regarding reaction time, the first maximum peak occurs at 5.00, 5.08 and 5.20 ms in the first phase when the medium viscosity is η = 0, 1 and 2 Pa·s, respectively. Similarly, the first maximum peak occurs at 110.38, 110.55 and 110.75 ms in the second phase when the medium viscosity is η = 0, 1 and 2 Pa·s, respectively. The period of oscillations and the reaction time increase with increasing medium viscosity. Overall, the results predicted by the proposed mathematical model here comply with the expected behaviors based on the literature [28], [35]–[38].

5 Experimental Validation

5.1 *Experimental study*

A hemisphere with a radius R located at the interface of the gelatin sample having a uniform shear modulus

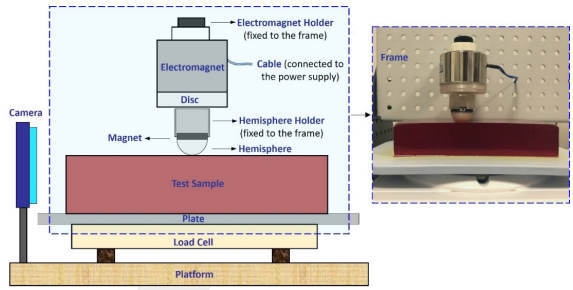

Figure 5: The schematic picture for the experimental setup (left panel) and the picture of the test setup (right panel).

G, density ρ, viscosity η and Poisson's ratio ν was pushed using a magnetic force (f) and the displacement of the hemisphere $u(t)$ was tracked using a high-speed camera. The gelatin sample was placed on a plate located on the load cell. The sensitivity of the load cell used to measure the force amplitude was 0.1 mN. A small cylindrical magnet was assembled to the top surface of the hemisphere to apply a force by an electromagnet (KK-P50/30 DC12V, Yueqing Kaka Electric Co. Ltd., China) to the hemisphere located at the sample interface. A power supply (GPS-3303, GW Instek, Taiwan) was used to operate the electromagnet in the experiments. The electromagnet was fixed to the frame using the electromagnet holder. The hemisphere holder fixed to the frame was used to eliminate the undesired rotation of the hemisphere. The schematic picture for the experimental setup and the picture of the test setup are shown in Figure 5. The videos were captured at 240 fps and the resolution was 0.06 mm/pixel. The displacement of the hemisphere from the videos as a function of time (t) was tracked using Matlab (MathWorks, Natick, MA, USA).

The radius and mass of the hemisphere were 12.15 mm and 4.06 g, respectively. The mass of the magnet was 10.97 g. Hence, the equivalent density of the spherical object was calculated to be ρ_s = 2000.51 kg/m^3. The total weight of the hemisphere and magnet was $\overline{F}_w$ = 147.4 mN. A gelatin sample was prepared by using 200 g gelatin and 600 g hot water (100 °C) and stored in the fridge at 4 °C for 4 h. The dimensions of the test sample were 37.7 × 155 × 210 mm^3. The density of the sample based on its measured mass and volume was ρ = 1105.16 kg/m^3. A second sample was prepared using 250 g gelatin and 600 g water (100 °C)

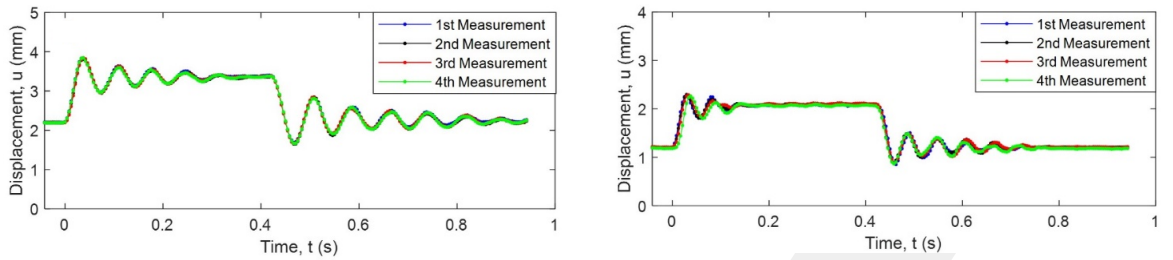

Figure 6: The four repeated experiments for (a) the first sample (ρ = 105.16 kg/m^3) and (b) the second sample (ρ = 1133.43 kg/m^3).

to further confirm the results. This sample was stored in stored in the fridge at 4 °C for 23 h. The dimensions and the density of this sample were 32.0 × 84.9 × 138.5 mm^3 and ρ = 1133.43 kg/m^3, respectively.

The displacement of the hemisphere placed at the interfaces of the first and second gelatin samples due to the weight of the hemisphere and magnet (i.e., 147.4 mN) was determined to be 2.2 and 1.2 mm, respectively. After the hemisphere at the sample surface was displaced by the initial loading, the electromagnet was operated for τ = 420 ms for both gelatin samples. The external force applied to the hemisphere by the electromagnet was $\overline{F}_m$ = 138.1±0.9 and 151.1 ± 0.4 mN for the first and second gelatin samples, respectively. All the experiments were performed at room temperature (24.6 °C). Four experiments were repeated for each test sample.

The four repeated experiments for each sample are presented in Figure 6. The experiments were highly repeatable, having a low standard deviation across measurements. The average deviation was 0.02 and 0.03 mm for the first and second gelatin samples, respectively. As the second sample was prepared using more gelatin powder and stored in the fridge for a longer duration, the second sample was expected to have higher shear modulus and viscosity. The results in Figure 6 show that the displacements were lower, and the oscillations decayed faster (in other words, the viscosity was higher) for the second sample. As the frequency of oscillations increases with stiffness (or shear modulus), the frequency of oscillations is higher (or the period of oscillations is lower) for the second sample.

As expected, once the electromagnet was operated, the hemisphere located at the sample interface (u = 2.2 and 1.2 mm for the first and second samples, respectively) first went down and reached the maximum displacement (u = 3.8 and 2.3 mm for the first and second samples, respectively), then its displacement decreased in time, and ultimately the hemisphere approached the steady-state condition (u = 3.4 and 2.1 mm for the first and second samples, respectively). Similarly, once the electromagnet stopped running, the hemisphere located at the sample interface went up and oscillated around its initial position (u = 2.2 and 1.2 mm for the first and second samples, respectively). The frequency of oscillations of the hemisphere placed at the interface of the first sample for the loading and unloading phases were 14.4 and 13.1 Hz, respectively. The corresponding values were 19.0 and 16.7 Hz, respectively, for the second sample. These experimental results show that the frequencies of oscillations of the hemisphere located at the medium interface are different in the loading and unloading phases. The weight of the sphere was large enough to maintain contact between the sphere and sample, hence it enabled measuring the response of the sphere during the relaxation phase.

5.2 *Comparison of the experimental data and mathematical model and discussion*

By minimizing the difference between the experimentally identified steady-state displacement in the loading phase and the steady-state displacement in the loading phase predicted by varying the value of the shear modulus of the material in the analytical model, the shear modulus was determined to be G = 3000 and 6800 Pa for the first and second samples, respectively. By minimizing the error between experimentally

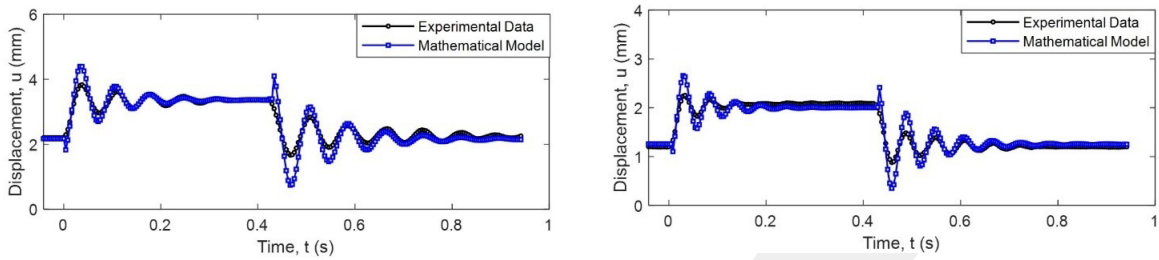

(a) (b)

Figure 7: The experimental and predicted responses of the hemisphere placed at the interface of (a) the first sample (ρ = 1105.16 kg/m^3) and (b) the second sample (ρ = 1133.43 kg/m^3).

identified amplitudes of oscillations in the loading phase and the amplitudes of oscillations in the loading phase predicted by varying the value of the viscosity of the material in the analytical model, the viscosity was determined to be η = 1.5 and 6.0 Pa·s for the first and second samples, respectively. The estimated response of the hemisphere placed at the interface of the sample using the identified shear modulus and viscosity and the other properties of the sample and hemisphere given before are compared with the average experimental response for both samples in Figure 7. The measured and predicted responses seem to fit well in the loading phase as well as in the relaxation phase for both samples.

The predicted frequency of oscillations was 14.4 Hz in the loading phase (being the same as the experimental one) and the predicted frequency of oscillations in the unloading phase was 12.9 Hz, which was close to the experimental one (13.1 Hz) for the first sample. The predicted frequencies of oscillations were 19.0 and 16.7 Hz in the loading and unloading phases, respectively, for the second sample. These frequencies were the same as the experimental ones. It is shown that the frequency of oscillations decreases as the external load decreases (in the unloading phase) and the mathematical model proposed here is able to simulate this.

Although the predicted amplitude of the first peak is higher than the measured one, the experimental and predicted amplitudes of oscillations are in general close to each other for both samples. For example, the experimental amplitudes of oscillations for the first four peaks and the steady-state displacement in the loading phase are 3.83, 3.62, 3.54, 3.47, and 3.37 mm, respectively for the first sample. The corresponding results for the same sample predicted by the model are 4.39, 3.78, 3.53, 3.43, and 3.37 mm, respectively. In general, the difference between the amplitudes of the measured and predicted first peaks is 10–15%, and the difference between all other measured and predicted peaks is less than 5% in the loading and relaxation phases.

It has been shown that the friction coefficient between a soft hydrogel and a hard sphere is negligible, even for high loads or sphere displacements, the corresponding viscosity is equal to or less than 0.1 Pa·s [28]. However, in our system, there were other sources of damping such as air friction, magnetic damping and the friction between the magnet and hemisphere holder. These sources of damping can be eliminated in future applications. The sharp changes at the time when the force is increased or decreased are seen in the results predicted by the mathematical model, though there are no sharp changes in the experimental results. First, the friction in the system can minimize these sharp changes in the experiments. Second, although an ideal rectangular pulse was assumed in the mathematical model, such an ideal pulse cannot be obtained in practice. Therefore, it is more appropriate to describe the temporal evolution of the magnetic force by a trapezoidal pulse with a finite ramp or rise time [32]. It is well known that the amplitude of the first peak decreases and the peak shifts to the right as the slope of the ramp decreases, compared to the ideal function with an infinity slope at the beginning, though the other peaks are slightly affected, and the steady-state displacement is not affected [32]. Some potential smoothing functions for the force can be included, or the mathematical models presented in this study can be easily updated using the expression of the trapezoidal

pulse used in [32] in future models. It is worth noting that, unlike other parameters such as shear modulus, the accurate modeling and experimentally identification of damping for almost any type of material is always challenging, as many parameters affect the damping of a system [11], [16], [17].

Overall, the measured and predicted natural frequencies and steady-state displacements for the loading and unloading phases and the identified material properties of the two gelatin phantoms are listed Table 1. Once again, it is seen that there is a negligible deviation between the experimental and predicted results in both the loading and the unloading phases. Additionally, the gelatin phantom with a higher gelatin ratio has a higher shear modulus and viscosity, and the natural frequency decreases as the external load decreases. The frequency of oscillations during loading is 10–15% higher than that during unloading.

It should be noted that measuring the properties of viscoelastic materials is challenging. Different loading cases have high practical value and the formulations for different loading cases can provide an accurate determination of material properties in a multitude of biomedical and industrial applications. For example, the procedure presented here can be used to accurately identify the shear modulus and viscosity of tissues and tissue-mimicking materials in practical applications [11], [40]. The procedure can even be exploited to identify the shear or Young's modulus and damping of green natural fiber samples that are needed in the prediction of their acoustic properties [41]–[43].

6 Conclusions

The motion of a spherical object located at the soft elastic and viscoelastic material interface for the identification of material properties was thoroughly investigated in this paper. Formulations for different loading practical cases were derived. The response of a spherical object located at elastic (no viscosity) medium interface was modeled by exploiting the forced vibrations of a system in the loading phase and the free vibrations of a system in the relaxation phase. The response of a spherical object located at a viscoelastic medium interface was determined by solving the equation of motion in the frequency domain, using the inverse Fourier transform. The measured and predicted responses of a spherical object located at a viscoelastic medium were compared and the viscoelastic material properties were identified in an experimental study. The experimental setup and the corresponding mathematical model presented here have wide practical applications. The mathematical model considers the weight of the spherical object, noting that the weight of the spherical object is typically not ignorable. The mathematical model takes into consideration the non-zero force during the unloading phase that is desired to maintain the contact between the sphere and medium, providing the measurement of the response of the spherical object at the interface during unloading. The mathematical model simulates the change in the frequency of oscillations of the spherical object located at the medium interface with the applied load.

Table 1: The measured and predicted natural frequencies and steady-state displacements for the loading and unloading phases and the identified material properties of the first (ρ = 1105.16 kg/m^3) and second (ρ = 1133.43 kg/m^3) gelatin phantoms

	Experimental Data		Mathematical Model		Identified Material Properties	
	Natural Frequency (Hz)	Steady-State Displacement (mm)	Natural Frequency (Hz)	Steady-State Displacement (mm)	Shear Modulus (Pa)	Viscosity (Pa·s)
First Sample (Loading)	14.4	3.4	14.4	3.4	3000	1.5
First Sample (Unloading)	13.1	2.2	12.9	2.2		
Second Sample (Loading)	19.0	2.1	19.0	2.0	6800	6.0
Second Sample (Unloading)	16.7	1.2	16.7	1.3		

The results predicted by the approach based on the forced vibrations of a system in the first phase and the free vibrations of a system in the second phase were similar to the results predicted by the approach based on solving the equation of motion written in the frequency domain, using the inverse Fourier transform, for the special case of zero viscosity. The analyses performed using a spherical object located at a viscoelastic medium interface showed that the amplitudes of oscillations decreased, the steady-state displacement did not change, the frequency of oscillations slightly decreased, and the reaction time increased with the increasing damping or viscosity of the sample, being in agreement with well-known behaviors of other damped systems in the literature.

By matching the experimental and predicted steady-state displacements and the amplitudes of oscillations of the spherical object located at the sample interface in the loading phase, the shear modulus and viscosity of the gelatin phantoms with a density of 1105.2 and 1133.4 kg/m^3 were determined to be 3000 and 6800 Pa and 1.5 and 6.0 Pa·s, respectively. As expected, the shear modulus and viscosity of the gelatin phantom with a higher gelatin ratio were higher. By comparing the experimental and predicted dynamic responses of the spherical object located at the sample interface using the identified material properties, we found that the experimental and predicted frequencies of oscillations in both the loading and unloading phases were the same or close to each other. Although there were some differences in the experimental and predicted amplitudes of the first peak, the amplitudes of oscillations in the loading and unloading phases were in general close to each other. Both the experimental and predicted results showed that the frequencies of oscillations were different in the loading and unloading phases, and the frequency of oscillations decreased with decreasing external load.

Acknowledgments

This work was supported by TUBITAK (The Scientific and Technological Research Council of Turkey) under Grant 1919B012102179 (application number). Hasan Koruk was supported by the Focused Ultrasound Foundation (grant number FUS1050R1) and the Little Princess Trust (grant number CCLGA 2022 25). We thank Hayati Omer Koc (BSc), Salih Berk Yurdaer (BSc) and Ayca Besli (BSc) for their support regarding the experiments.

Author Contributions

H.K.: conceptualization; research design; investigation; methodology; data analysis; writing, reviewing & editing; funding acquisition; and project administration; A.N.P.: investigation; reviewing & editing; and funding acquisition. All authors have read and agreed to the published version of the manuscript.

Conflicts of Interest

The authors declare no conflicts of interest.

References

[1] Y. A. Ilinskii, G. D. Meegan, E. A. Zabolotskaya, and S. Y. Emelianov, "Gas bubble and solid sphere motion in elastic media in response to acoustic radiation force," *The Journal of the Acoustical Society of America*, vol. 117, no. 4, pp. 2338–2346, 2005, doi: 10.1121/1.1863672.

[2] S. R. Aglyamov, A. B. Karpiouk, Y. A. Ilinskii, E. A. Zabolotskaya, and S. Y. Emelianov, "Motion of a solid sphere in a viscoelastic medium in response to applied acoustic radiation force: Theoretical analysis and experimental verification," *The Journal of the Acoustical Society of America*, vol. 122, no. 4, pp. 1927–1936, 2007, doi: 10.1121/1.2774754.

[3] C.-C. Huang, C.-C. Shih, T.-Y. Liu and P.-Y. Lee, "Assessing the viscoelastic properties of thrombus using a solid-sphere-based instantaneous force approach," *Ultrasound in Medicine & Biology*, vol. 37, no. 10, pp. 1722–1733, 2011, doi: 10.1016/j.ultrasmedbio.2011.06.026.

[4] S. Yoon, S. R. Aglyamov, A. B. Karpiouk, S. Kim, and S. Y. Emelianov, "Estimation of mechanical properties of a viscoelastic medium using a laser-induced microbubble interrogated by an acoustic radiation force," *The Journal of the Acoustical Society of America*, vol. 130, no. 4, pp. 2241–2248, 2011, doi: 10.1121/1.3628344.

[5] S. Yoon, S. Aglyamov, A. Karpiouk, and S. Emelianov, "The mechanical properties of ex vivo bovine and porcine crystalline lenses:

Age-related changes and location-dependent variations," *Ultrasound in Medicine & Biology*, vol. 39, no. 6, pp. 1120–1127, 2013, doi: 10.1016/j.ultrasmedbio.2012.12.010.

[6] B. E. Levy and A. L. Oldenburg, "Single magnetic particle motion in magnetomotive ultrasound: An analytical model and experimental validation," *IEEE Transactions on Ultrasonics, Ferroelectrics, and Frequency*, vol. 68, no. 8, pp. 2635–2644, 2021, doi: 10.1109/TUFFC.2021.3072867.

[7] A. Cebrecos, N. Jiménez, R. Tarazona, M. Company, J. M. Benlloch, and F. Camarena, "Characterization of viscoelastic media combining ultrasound and magnetic-force induced vibrations on an embedded soft magnetic sphere," *IEEE Transactions on Ultrasonics, Ferroelectrics, and Frequency*, vol. 68, no. 12, pp. 3540–3548, 2021, doi: 10.1109/TUFFC.2021.3097883.

[8] H. Koruk, A. E. Ghamrawy, A. N. Pouliopoulos, and J. J. Choi, "Acoustic particle palpation for measuring tissue elasticity," *Applied Physics Letters*, vol. 107, no. 22, 2015, Art. no. 223701, doi: 10.1063/1.4936345.

[9] H. Koruk and J. J. Choi, "Displacement of a bubble by acoustic radiation force into a fluid–tissue interface," *The Journal of the Acoustical Society of America*, vol. 143, no. 4, pp. 2535–2540, 2018, doi: 10.1121/1.5034175.

[10] H. Koruk and J. J. Choi, "Displacement of a bubble located at a fluid-viscoelastic medium interface," *The Journal of the Acoustical Society of America*, vol. 145, no. 5, pp. EL410–EL416, 2019, doi: 10.1121/1.5108678.

[11] J. H. Bezer, H. Koruk, C. J. Rowlands, and J. J. Choi, "Elastic deformation of soft tissue-mimicking materials using a single microbubble and acoustic radiation force," *Ultrasound in Medicine & Biology*, vol. 46, no. 12, pp. 3327–3338, 2020, doi: 10.1016/j.ultrasmedbio.2020.08.012.

[12] H. Koruk, "Assessment of the models for predicting the responses of spherical objects in viscoelastic mediums and at viscoelastic interfaces," *IOP Conference Series: Materials Science and Engineering*, vol. 1150, 2021, Art. no. 012016, doi: 10.1088/1757-899X/1150/1/012016.

[13] H. Koruk, "Development of a model for predicting dynamic response of a sphere at viscoelastic interface: A dynamic Hertz model," *IOP Conference Series: Materials Science and Engineering*, vol. 1150, 2021, Art. no. 012015, doi: 10.1088/1757-899X/1150/1/012015.

[14] H. Koruk, A. Besli, H. O. Koc, and S. B. Yurdaer, "Identification of material viscoelastic properties using the motion of a rigid sphere located at tissue-mimicking material interface in response to a dynamic force," *Materials Science Forum*, vol. 1066, pp. 73–78, 2022, doi: 10.4028/p-oum2c1.

[15] H. Koruk, S. B. Yurdaer, H. O. Koc, and A. Besli, "Identification of the viscoelastic properties of soft materials using a convenient dynamic indentation system and procedure," *Materials Today: Proceedings*, vol. 57, part 2, pp. 464–468, 2022, doi: 10.1016/j.matpr.2022.01.188.

[16] H. Koruk and K. Y. Sanliturk, "Identification and removal of adverse effects of non-contact electromagnetic excitation in Oberst Beam Test Method," *Mechanical Systems and Signal Processing*, vol. 30, pp. 274–295, 2012, doi: 10.1016/j.ymssp.2012.02.003.

[17] K. Y. Sanliturk and H. Koruk, "A new triangular composite shell element with damping capability," *Composite Structures*, vol. 118, pp. 322–327, 2014, doi: 10.1016/j.compstruct.2014.07.053.

[18] H. Koruk and K. Y. Sanliturk, "Optimisation of damping treatments based on big bang-big crunch and modal strain energy methods," *Journal of Sound and Vibration*, vol. 333, no. 5, pp. 1319–1330, 2014, doi: 10.1016/j.jsv.2013.10.023.

[19] H. Koruk, "Quantification and minimization of sensor effects on modal parameters of lightweight structures," *Journal of Vibroengineering*, vol. 16, no. 4, pp. 1952–1963, 2014.

[20] X. Zhang, B. Qiang, and J. Greenleaf, "Comparison of the surface wave method and the indentation method for measuring the elasticity of gelatin phantoms of different concentrations," *Ultrasonics*, vol. 51, no. 2, pp. 157–164, 2011, doi: 10.1016/j.ultras.2010.07.005.

[21] R. Han and J. Chen, "A modified Sneddon model for the contact between conical indenters and spherical samples," *Journal of Materials Research*, vol. 36, pp. 1762–1771, 2021, doi: 10.1557/s43578-021-00206-5.

[22] S. V. Kontomaris, A. Georgakopoulos, A. Malamou, and A. Stylianou, "The average Young's modulus as a physical quantity for describing the depth-

dependent mechanical properties of cells," *Mechanics of Materials*, vol. 158, 2021, Art. no. 103846, doi: 10.1016/j.mechmat.2021.103846.

[23] D. Xu, T. Harvey, E. Begiristain, C. Domínguez, L. Sánchez-Abella, M. Browne, and R. B. Cook, "Measuring the elastic modulus of soft biomaterials using nanoindentation," *Journal of the Mechanical Behavior of Biomedical Materials*, vol. 133, 2022, Art. no. 105329, doi: 10.1016/j.jmbbm.2022.105329.

[24] S. V. Kontomaris, A. Stylianou, A. Malamou, and K. S. Nikita, "An alternative approach for the Young's modulus determination of biological samples regarding AFM indentation experiments," *Materials Research Express*, vol. 6, 2019, Art. no. 025407, doi: 10.1088/2053-1591/aaef10.

[25] L. Cheng, X. Xia, L. E. Scriven, and W. W. Gerberich, "Spherical-tip indentation of viscoelastic material," *Mechanics of Materials*, vol. 37, no. 1, pp. 213–226, 2005, doi: 10.1016/j.mechmat.2004.03.002.

[26] B. Qiang, J. Greenleaf, M. Oyen, and X. Zhang, "Estimating material elasticity by spherical indentation load-relaxation tests on viscoelastic samples of finite thickness," *IEEE Transactions on Ultrasonics, Ferroelectrics, and Frequency*, vol. 58, no. 7, pp. 1418–1429, 2011, doi: 10.1109/TUFFC.2011.1961.

[27] I. Argatov and G. Mishuris, *Indentation Testing of Biological Materials*. Cham: Springer, 2018, doi: 10.1007/978-3-319-78533-2.

[28] M. Mizukami, H. -Y. Ren, H. Furukawa, and K. Kurihara, "Deformation of contacting interface between polymer hydrogel and silica sphere studied by resonance shear measurement," *The Journal of Chemical Physics*, vol. 149, no. 16, 2018, Art. no. 163327, doi: 10.1063/1.5037326.

[29] S. -V. Kontomaris and A. Malamou, "Exploring the non-linear oscillation of a rigid sphere on an elastic half-space," *European Journal of Physics*, vol. 42, no. 2, 2021, Art. no. 025011, doi: 10.1088/1361-6404/abce1d.

[30] H. Koruk, "Modelling small and large displacements of a sphere on an elastic half-space exposed to a dynamic force," *European Journal of Physics*, vol. 42, no. 5, 2021, Art. no. 055006, doi: 10.1088/1361-6404/ac0e42.

[31] H. Koruk, "Development of an improved mathematical model for the dynamic response of a sphere located at a viscoelastic medium interface," *European Journal of Physics*, vol. 43, no. 2, 2022, Art. no. 025002, doi: 10.1088/1361-6404/ac4647.

[32] H. Koruk, H. O. Koc, S. B. Yurdaer, A. Besli, and A. N. Pouliopoulos, "A new approach for measuring viscoelastic properties of soft materials using the dynamic response of a spherical object placed at the sample interface," *Experimental Mechanics*, 2023, doi: 10.1007/s11340-023-01004-2.

[33] D. J. Inman, *Engineering Vibrations*. New Jersey: Pearson Education, 2013.

[34] S. Chen, M. W. Urban, C. Pislaru, R. Kinnick, Y. Zheng, A. Yao, and J. F. Greenleaf, "Shearwave dispersion ultrasound vibrometry (SDUV) for measuring tissue elasticity and viscosity," *IEEE Transactions on Ultrasonics, Ferroelectrics, and Frequency*, vol. 56, no. 1, pp. 55–62, 2009, doi: 10.1109/TUFFC.2009.1005.

[35] S. H. Crandall, "The role of damping in vibration theory," *Journal of Sound and Vibration*, vol. 11, no. 1, pp. 3–18, 1970, doi: 10.1016/S0022-460X(70)80105-5.

[36] J. P. Holman, *Experimental Methods for Engineers*. New York: McGraw Hill, 2012.

[37] H. Koruk, J. T. Dreyer, and R. Singh, "Modal analysis of thin cylindrical shells with cardboard liners and estimation of loss factors," *Mechanical Systems and Signal Processing*, vol. 45, no. 2, pp. 346–359, 2014, doi: 10.1016/j.ymssp.2013.10.026.

[38] H. Koruk and K. Y. Sanliturk, "A novel definition for quantification of mode shape complexity," *Journal of Sound and Vibration*, vol. 332, no. 14, pp. 3390–3403, 2013, doi: 10.1016/j.jsv.2013.01.039.

[39] B. D. Siva Deeraj, K. Joseph, J. S. Jayan, and A. Saritha, "Dynamic mechanical performance of natural fiber reinforced composites: A brief review," *Applied Science and Engineering Progress*, vol. 14, no. 4, pp. 614–623, 2021, doi: 10.14416/j.asep.2021.06.003.

[40] A. E. Ghamrawy, F. de Comtes, H. Koruk, A. Mohammed, J. R. Jones, and J. J. Choi, "Acoustic streaming in a soft tissue microenvironment," *Ultrasound in Medicine & Biology*, vol. 45, no. 1, pp. 208–217, 2019, doi: 10.1016/j.ultrasmedbio.2018.08.026.

[41] A. C. Ozcan, K. Y. Sanliturk, G. Genc, and H. Koruk, "Investigation of the sound absorption and transmission loss performances of green homogenous and hybrid luffa and jute fiber samples," *Applied Science and Engineering Progress*, vol. 14, no. 4, pp. 668–679, 2021, doi: 10.14416/j.asep.2021.04.005.

[42] H. Koruk, "Assessment of the measurement and prediction methods for the acoustic properties of natural fiber samples and evaluation of their properties," *Journal of Natural Fibers*, vol. 19, no. 13, pp. 6283–6311, 2022, doi: 10.1080/15440478.2021.1907835.

[43] S. M. Rangappa, S. Siengchin, and H. N. Dhakal, "Green-composites: Ecofriendly and sustainability," *Applied Science and Engineering Progress*, vol. 13, no. 3, pp. 183–184, 2020, doi: 10.14416/j.asep.2020.06.001.